International Journal of Fracture, Vol. 18, No. 4, April 1982

The Hague, The Netherlands

Combined mode fracture via the cracked Brazilian disk test

C. ATKINSON* (Visiting Professor), R. E. SMELSER and J. SANCHEZ**

Mechanical Engineering Department, University of Pittsburgh, Pittsburgh, PA 15261, USA

(Received December 19, 1980)

ABSTRACT

An analysis is made of the cracked Brazilian disk test. Explicit results are given for the stress intensity factors of a crack aligned at any direction to the applied load. Various approximations are considered and a simplified 'short crack' approximation is shown to be accurate for $\ell/a \leq 0.3$ (ℓ is crack length, a the disk radius). At certain angles it is found that crack closure should occur and as a first step the effect of friction is taken into account for such cases by using this short crack approximation. Finally, experimental results are presented to confirm and elucidate the use of this specimen geometry for the problem of combined mode fracture.

1. Introduction

Recently, a series of papers by Eftis *et al.* [1, 2, 3] has re-examined the problem of an inclined crack in a plate under remote biaxial loading. Their purpose was to demonstrate the effect of remote stresses and load biaxiality on K_I and K_{II} as well as the effect on various fracture criteria. A critical review of the various fracture criteria has been given by Swedlow [4]. Here it is pointed out that the existing test data do not allow any selection to be made between the various competing criteria, and it is recommended that alternative tests be considered as well as an expansion of the data base for combined mode fracture.

It is in this latter area where the current specimen would seem to be most useful. The specimen geometry is shown in Fig. 1 and is a variant of the early work of Libatskii and Kovshik [5] and Yarema and Krestin [6]. The specimen of Fig. 1 has been investigated by Ajawi and Sato [7] and by Sanchez [8] as an alternative to the compact shear specimen of Jones and Chisholm [9, 10]. In addition to the determination of K_{IIC}, Awaji and Sato [7] also examined the possibility of the existence of a fracture criterion in the form

$$\left(\frac{K_I}{K_{IC}}\right)^u + \left(\frac{K_{II}}{K_{IIC}}\right)^u = 1. \tag{1.1}$$

In contrast to the numerical analyses of [7, 8], we present explicit formulae for K_I and K_{II} valid for any angle of crack orientation in the cracked Brazilian disk test, Eqn. (3.1). Also, an approximate analysis valid for short cracks is given, and the effect of friction is included when crack closure is present. Finally, experimental results are presented which demonstrate the feasibilityof producing short cracks in moderate size specimens, thus indicating the usefulness of the approximate analysis and of the specimen geometry in expanding and elucidating the problem of combined mode fracture.

* Permanent Address: Imperial College, London, U.K.

** Now with: Universidad del Valle Cali, Colombia.

0376-9429/82/040279-13$00.20/0

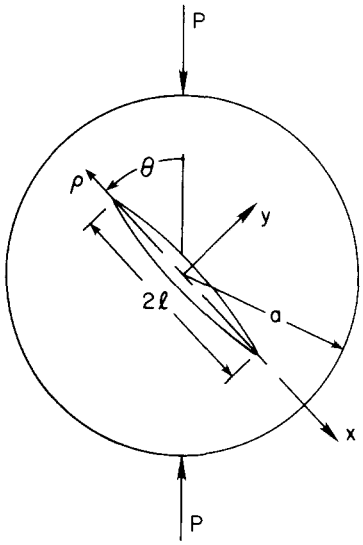

Figure 1. Geometry of the cracked Brazilian disk test.

2. Analysis

To give a complete numerical treatment of the problem, we follow a method outlined by Atkinson [11]. The crack is represented by a continuous distribution of edge dislocations, simulating discontinuities in the normal and tangential components of displacement. Because the crack lies on a diameter of the disc, there is no interaction between dislocations representing discontinuities in the normal displacement and those representing discontinuities in the tangential displacement. The tractions on the axis $y = o$ due to the unknown distribution of dislocations can be written in the form

$$\frac{\sigma_{i2}}{D} = \int_{\ell}^{\ell} \frac{N_i(c)\,dc}{x-c} + \int_{\ell}^{\ell} N_i(c) H_i(c,x)\,dc \quad i = 1,2 \tag{2.1}$$

The precise form for $H_i(c, x)$ can be deduced from [12] where the case of a circular inclusion was considered. Note, however, a misprint in equation (2.2.2) of [12]). The factor in the last term in the curly brackets should be $2/\beta a$ not $X^2/\beta a$. In (2.1), $D = 2G/(\kappa + 1)$, G is the shear modulus, and $\kappa = 3 - 4\nu$ (plane strain) or $\kappa = (3-\nu)/(1+\nu)$ (plane stress) ν being poisson's ratio. For convenience, we have taken the Burgers vector, b, to be unity. The corresponding opening of the crack faces can be written

$$\Delta u_i = \int_{x}^{\ell} N_i(c)\,dc \quad i = 1,2 \tag{2.2}$$

where (u_1, u_2) are the (x, y) components of the displacement, and σ_{ij} is the usual stress tensor. The subsidiary conditions

$$\int_{-\ell}^{\ell} N_i(c)\,dc = 0 \quad i = 1,2 \tag{2.3}$$

ensure that the crack closes at the ends $(\pm\ell, o)$.

The distributions $N_i(c)$ are to be determined from the condition that the crack be stress free and that it closes at the ends (condition (2.3)). The first of these conditions is met by replacing σ_{i2} in (2.1) by minus the stress induced on the crack line ($|x| \leq \ell$,

$y = o$) by the applied stresses set up in the disc in the absence of the crack. Complete expressions for these stresses are given in Appendix 1. For the moment, we assume the stress is represented by

$$\sigma_{i2}(x) = -\sigma_i(x) \quad i = 1, 2 \tag{2.4}$$

given on $y = o$, $|x| \leq \ell$. Equation (2.1) then becomes an integral equation for the unknown densities $N_i(c)$.

Two methods of treating this equation numerically are given in [11]. One of these methods consists of solving (2.1) directly by expanding (2.1) in terms of Chebyschev polynamials. The other method consists of first transforming (2.1) into a Fredholm equation and then solving it numerically. We use the latter method here since it is possible to express the kernel in closed form.

Using (2.4) in (2.1) and inverting the singular integral, the resulting Fredholm equation can be written (see Atkinson [11])

$$N_{i1}(\eta) = \frac{-1}{\pi^2(1-\eta^2)^{1/2}}\left[\int_{-1}^{1} \frac{\sigma_i(\ell x_1)(1-x_1^2)^{1/2}}{x_1 - \eta}\,dx_1 + \right.$$
$$\left. + \int_{-1}^{1} N_{i1}(c_1)F_i(c_1, \eta)\,dc_1\right] \quad i = 1, 2 \tag{2.5}$$

where $c = \ell c_1$, $a = \ell a_1$, $x = \ell x_1$,

$$F_i(c_1, \eta) = \int_{-1}^{1} \frac{H_i(\ell c_1, \ell x_1)(1-x_1^2)^{1/2}}{x_1 - \eta}\,dx_1$$

and $N_{i1}(\eta) = N_i(\ell\eta)$. Making these coordinate transformations in (2.2), gives

$$\Delta u_i(x, o) = \ell \int_{x_1}^{1} N_{i1}(c_1)\,dc_1. \tag{2.6}$$

We expect $N_{i1}(\eta)$ to have inverse square root singularities at $\eta = \pm 1$, so we write

$$N_{i1}(\eta) = N_{io}(\eta)(1-\eta^2)^{-1/2} \tag{2.7}$$

Now make the substitutions $\eta = \cos\alpha$, $c_1 = \cos\psi$ and $x_1 = \cos\psi_1$ so that Eqns. (2.5) become

$$N_{io}(\cos\alpha) = \frac{-1}{\pi^2}\left[f(\cos\alpha) + \int_0^{\pi} N_{io}(\cos\psi)F_i(\cos\psi, \cos\alpha)\,d\psi\right] \tag{2.8}$$

for $0 \leq \alpha \leq \pi$. $f(\cos\alpha)$ is to be derived from the first integral on the right of (2.5). Note that $F_i(\cos\psi, \cos\alpha)$ can be expressed in closed form by completing the integral following (2.5).

The next step in the solution of the problem is to replace the integral in (2.8) as a sum and solve the resulting system of simultaneous equations. Once this is done, substituting into (2.6) shows that

$$\Delta u_i(x, o) = (2\ell)^{1/2}N_{io}(1)(\ell - x)^{1/2} \tag{2.9}$$

as $x \to \ell_-$. Furthermore, from (2.2), the crack opening displacements along the crack flanks can be computed as

$$\Delta u_i(x, o) = \ell \int_0^{\psi_1} N_{io}(\cos\psi)\,d\psi \tag{2.10}$$

where $\psi_1 = \cos^{-1}(x/\ell)$.

3. Results

The analysis of Section 2 may be used to determine the stress intensity factors associated with cracks of varying length and orientation. Such a determination requires the evaluation of $f(\cos\alpha)$ in (2.8). $f(\cos\alpha)$ may be evaluated through an expansion of $\sigma_i(x)$ in terms of Chebyschev polynomials and then numerically integrating to determine $f(\cos\alpha)$. This procedure is numerically sensitive. Thus an alternate method of evaluating $f(\cos\alpha)$ was used. Each term in the approximate stress distributions given in Appendix 1 may be independently used as input for (2.8). The resulting $N_{io}(1)$'s yield series approximations to the stress intensity factors in the form

$$N_{\mathrm{I}} = \sum_{i=1}^{n} T_i \left(\frac{\ell}{a}\right)^{2i-2} A_i(\theta)$$

$$N_{\mathrm{II}} = 2\sin 2\theta \sum_{i=1}^{n} S_i \left(\frac{\ell}{a}\right)^{2i-2} B_i(\theta) \tag{3.1}$$

where $N_{\mathrm{I}} = (K_{\mathrm{I}})/\sigma_o\sqrt{\pi\ell}$, $N_{\mathrm{II}} = (K_{\mathrm{II}})/\sigma_o\sqrt{\pi\ell}$ are normalized stress intensities and $\sigma_o = P/\pi a$. The T_i's and S_i's in (3.1) are numerical factors determined through the solution of (2.8). The first five values of T_i and S_i and the corresponding $A_i(\theta)$'s and $B_i(\theta)$'s are given in Tables 1 and 2 respectively.

TABLE 1
First five coefficients for (3.1)

ℓ/a	T_1 S_1	T_2 S_2	T_3 S_3	T_4 S_4	T_5 S_5
0.1	1.014998	0.503597	0.376991	0.376991	0.314159
	1.009987	0.502341	0.376363	0.376363	0.314159
0.2	1.060049	0.514907	0.382430	0.383392	0.318086
	1.039864	0.509959	0.379956	0.380584	0.316245
0.3	1.135551	0.533477	0.391640	0.393835	0.325033
	1.089702	0.522272	0.386086	0.387518	0.320834
0.4	1.243134	0.559734	0.404603	0.408597	0.334831
	1.160796	0.539824	0.394822	0.397403	0.327411
0.5	1.387239	0.594892	0.421949	0.428353	0.347941
	1.257488	0.563966	0.406869	0.410966	0.336447
0.6	1.578258	0.642124	0.445387	0.454861	0.365559
	1.390654	0.597985	0.424037	0.430072	0.349219

TABLE 2
First five angular constants for (3.1)

A_1	$1-4s^2$
A_2	$8s^2(1-4c^2)$
A_3	$-4s^2(3-36c^2+48c^4)$
A_4	$-16s^2(-1+24c^2-80c^4+64c^6)$
A_5	$-20s^2(1-40c^2+240c^4-448c^6+256c^8)$
B_1	1
B_2	$-5+8c^2$
B_3	$-3+8(1-2c^2)(2-3c^2)$
B_4	$3+16(1-2c^2)-12(1-2c^2)^2-32(1-2c^2)^3$
B_5	$5-16(1-2c^2)-60(1-2c^2)^2+32(1-2c^2)^3+80(1-2c^2)^4$

Note: $s = \sin\theta$; $c = \cos\theta$; $\cos 2\theta = 2c^2 - 1$

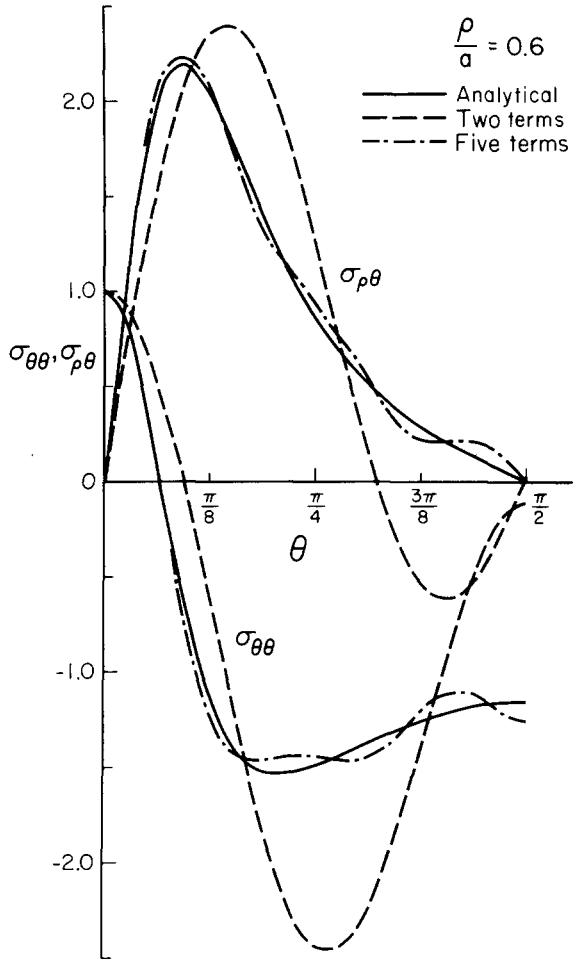

Figure 2. Stress distributions in the uncracked disk for $\rho/a = 0.6$.

The normalized uncracked disk stress distributions, $\sigma_{\theta\theta} = (\bar{\sigma}_{\theta\theta})/\sigma_o$ and $\sigma_{\rho\theta} = (\bar{\sigma}_{\rho\theta})/\sigma_o$ for $\rho/a = 0.6$ are shown in Fig. 2. As can be seen, the two term approximation yields a stress distribution greatly differing from the analytical solution. However, the approximation improves for small ρ/a, Fig. 3. The stress distributions of Fig. 2 produce only small differences in stress intensity factors as evidenced in Fig. 4. Here $N_{\rm I}$ and $N_{\rm II}$ for the two and five term approximations for $\ell/a = 0.5$ are compared with the numerical results of Awaji and Sato [7]. For the five term approximations, no discernible differences can be detected in the results, while the two term approximation shows differences of less than ten percent. This small difference for the two term approximation is due to the dominance of the first term on the expansion. In addition, Fig. 4 also ontains a series of finite element calculations due to Sanchez [8]. These results were obtained using a special crack tip element of Tong *et al.* [13] in a mesh of constant strain elements. The computations are seen to be in agreement with the other numerical results for the coarse mesh of Fig. 5.

Figure 4 shows that as the crack changes its orientation from the vertical to the horizontal the normalized stress intensity factor $N_{\rm I}$ changes from positive to negative indicating crack closure. At the point of crack closure, the model of the crack must be altered. This point was not considered in [7] and in general has not been incorporated

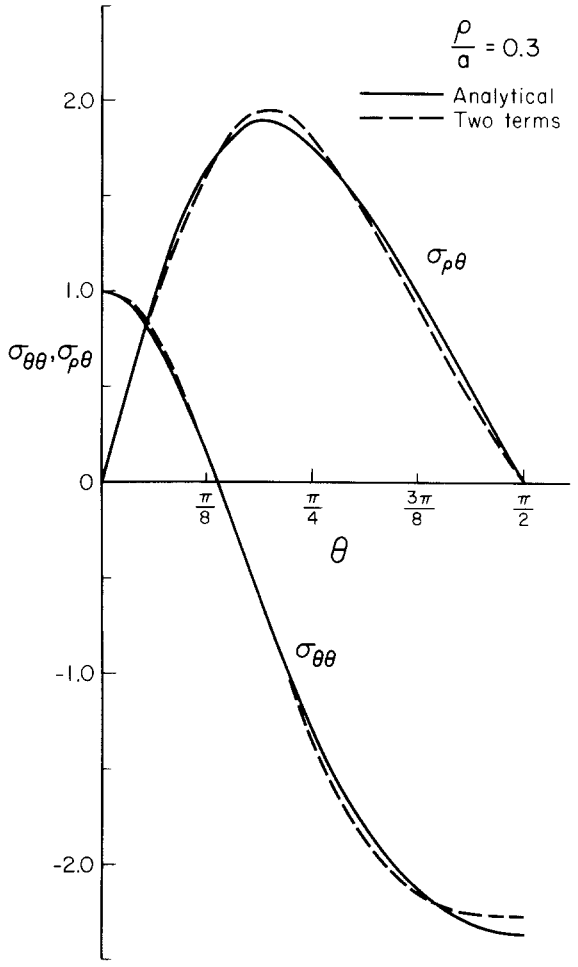

Figure 3. Stress distributions in the uncracked disk for $\rho/a = 0.3$.

in problems of mixed mode fracture [1–3]. Condition (2.2) must be modified so that

$$\Delta u_2 = 0 \tag{3.2}$$

for $\ell^* \leq |x| \leq \ell$ where ℓ^* is the position at which the crack first closes and $0 \leq \ell^* < \ell$ on $y = 0$. Now if Δu_2 is zero, an additional traction, $\sigma_{12}^*(x)$, is developed along the crack surface due to friction

$$\sigma_{12}^*(x) \leq \mu\sigma_{22}(x). \tag{3.3}$$

In the following section, an analysis for short cracks is presented and the effect of friction is incorporated.

4. Small crack approximation

If the crack length is small relative to the radius, then the second term on the right of (2.1) may be neglected, and the problem treated as a crack in an infinite media. Equation (2.1) becomes

$$\frac{\sigma_{i2}}{D} = \int_{-\ell}^{\ell} \frac{N_i(c)\,dc}{x - c} \quad i = 1, 2. \tag{4.1}$$

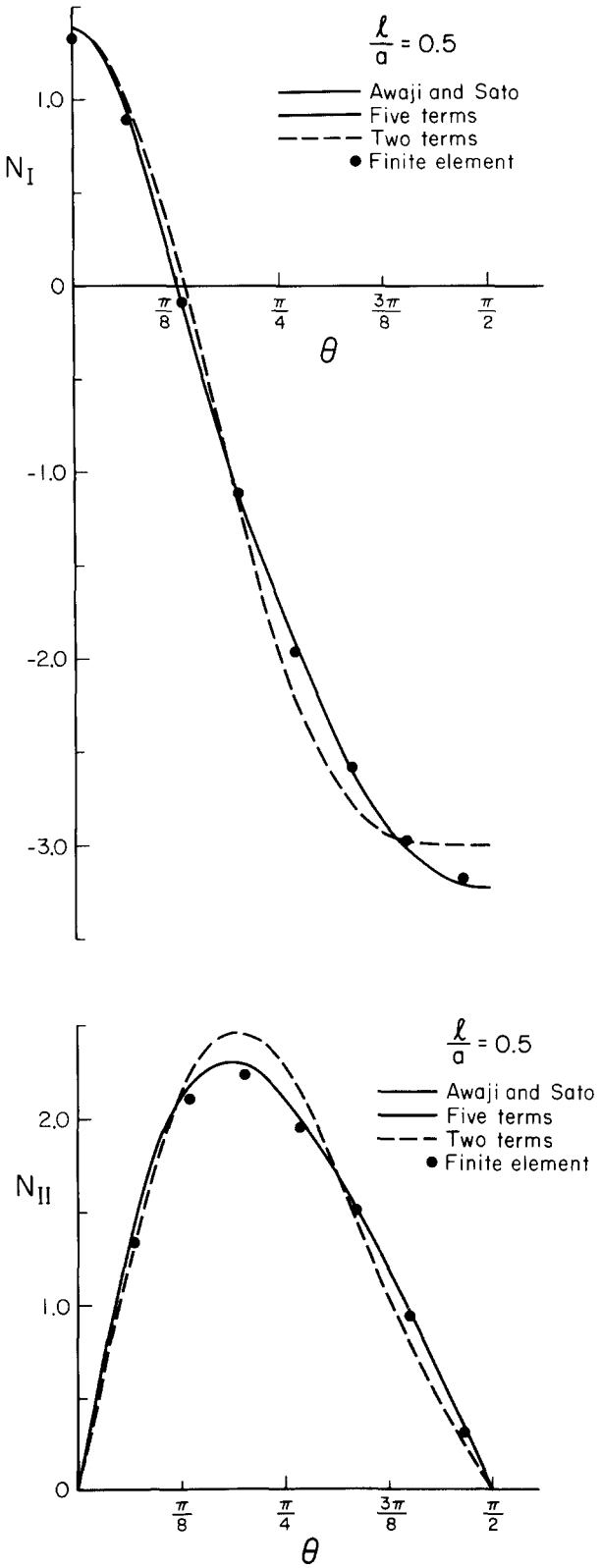

Figure 4. Stress intensity factors for $\ell/a = 0.5$ a) N_I, b) N_{II}.

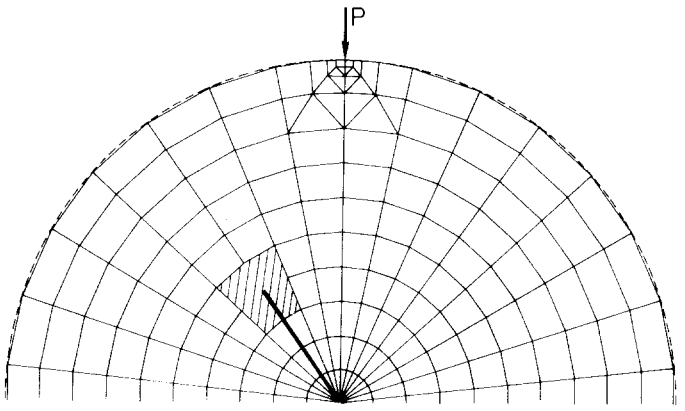

Figure 5. Finite element mesh for stress intensity factor determination.

Now from Appendix 1, the normal and shear stresses along the crack line are approximately

$$\bar{\sigma}_{22}(x) = \frac{P}{\pi a}\left[A_1 + A_2\left(\frac{x}{a}\right)^2\right]$$

$$\bar{\sigma}_{12}(x) = \frac{2P\sin 2\theta}{\pi a}\left[B_1 + B_2\left(\frac{x}{a}\right)^2\right] \tag{4.2}$$

since $x = \rho$ on $y = 0$. $\bar{\sigma}_{22}(x)$ and $\bar{\sigma}_{12}(x)$ are even functions of x, and the normalized stress intensity factors may be written as

$$N_{\mathrm{I}} = \frac{1}{\sigma_o \pi}\int_{-\ell}^{\ell} \frac{\sigma_{22}(x)\,dx}{(\ell^2 - x^2)^{1/2}}$$

$$N_{\mathrm{II}} = \frac{1}{\sigma_o \pi}\int_{-\ell}^{\ell} \frac{\sigma_{12}(x)\,dx}{(\ell^2 - x^2)^{1/2}}. \tag{4.3}$$

[Note, N_{I} and N_{II} are not to be confused with the dislocation densities $N_i(c)$.] Substituting (4.2) into (4.3) and integrating yields explicitly

$$N_{\mathrm{I}} = A_1 + \frac{A_2}{2}\left(\frac{\ell}{a}\right)^2$$

$$N_{\mathrm{II}} = \left[B_1 + \frac{B_2}{2}\left(\frac{\ell}{a}\right)^2\right] 2\sin 2\theta. \tag{4.4}$$

A comparison of expressions (4.4) with expressions (3.1) and the finite element results are given in Fig. 6 with $\ell/a = 0.3$. The approximations of (4.4) are seen to be quite good.

TABLE 3
Angles for pure mode II behavior for various crack lengths

ℓ/a	Eqn (4.5)	Sanchez [8]	Awaji and Sato [7]
0.3	27.2	27.7	27.2
0.4	25.4	25.2	25.2
0.5	23.3	23.2	22.9
0.6	21.3	20.0	20.1

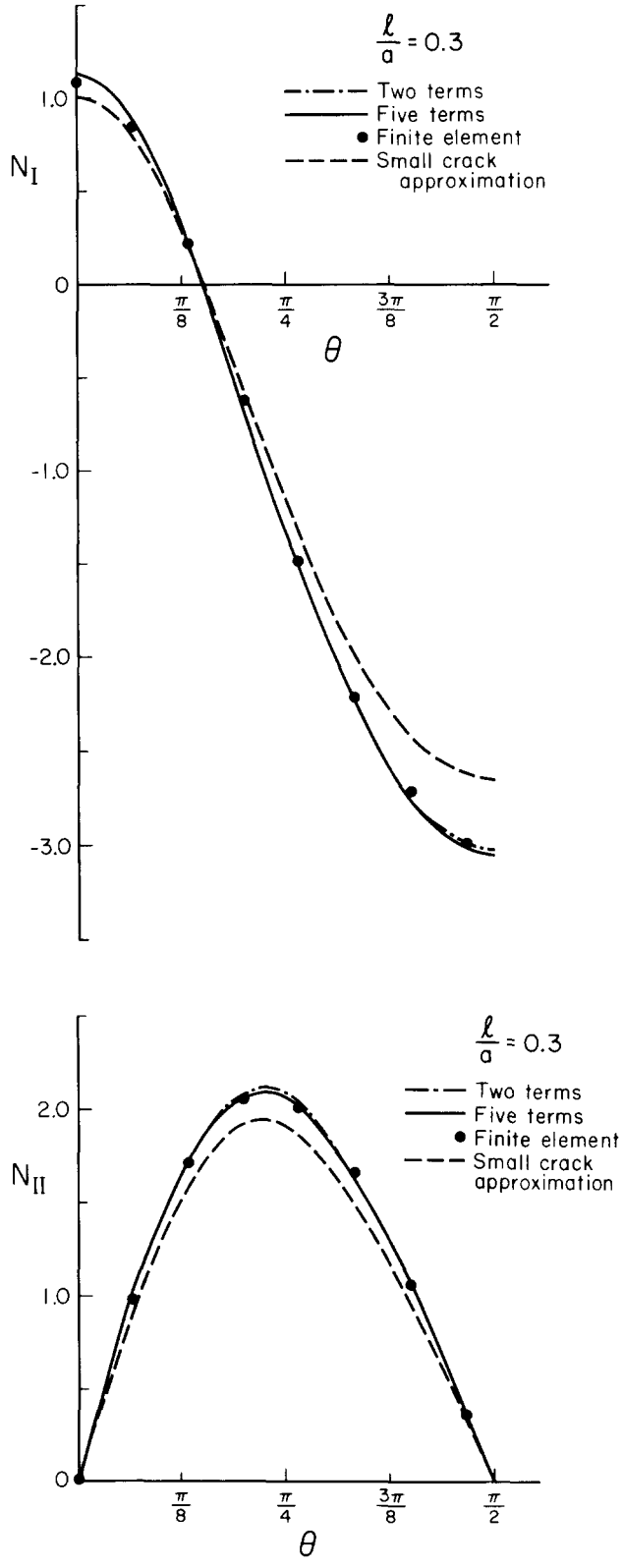

Figure 6. Stress intensity factors for the small crack approximation a) N_I, b) N_{II}.

From $(4.4)_1$ we may obtain an explicit equation for the angle at which the crack just begins to close

$$N_I = A_1 + \frac{A_2}{2}\left(\frac{\ell}{a}\right)^2 = 0. \tag{4.5}$$

This expression has been evaluated for fixed values of ℓ/a, and the results are compared with those of [7, 8] in Table 3. For angles of inclination greater than those in Table 3, the crack closes over some portion of its surface and a frictional stress is developed.

If in (4.5) θ is fixed in deference to ℓ/a, we obtain an equation for the position, ℓ^*, at which the crack closes. Now eqns (4.4) obtain for $\ell \leq \ell^*$. If $\ell \geq \ell^*$, we have in addition to the stress intensity factor N_{II} given by $(4.4)_2$ an additional contribution due to the frictional stress. We note that this is true even if N_I is constrained from being negative by imposing $\Delta u_2 = 0$ on $y = 0$ for $0 \leq \ell^* \leq |x| \leq \ell$. Additionally, this is true in the general case since there is no interaction between the normal and shear dislocations.

To evaluate the additional contribution to N_{II}, we must evaluate the stresses in the region $\ell^* \leq |x|$. The stresses ahead of the crack in this small crack approximation are given by

$$\frac{\sigma_{22}(x)}{D} = -\int_{-\ell^*}^{\ell^*} \frac{N_2^*(c)\,dc}{c - x}. \tag{4.6}$$

The $N_2^*(c)$ can be determined from the first term on the right hand side of (2.5) provided we replace ℓ by ℓ^*, $\ell^*\eta$ by c and use expression $(4.2)_1$ for $\sigma_i(x)$ with the condition that $\Delta u_2 = 0$ on $y = 0$ $|x| > \ell^*$. Equation (4.6) may then be evaluated to give, for $|x| > \ell^*$

$$\sigma_{22}(x) = \frac{\sigma_o x}{\sqrt{x^2 - \ell^{*2}}}\left[A_1 + \frac{A_2}{a^2}\left(x^2 - \frac{\ell^{*2}}{2}\right)\right] \tag{4.7}$$

and the friction stress within the contack zone is given by

$$\sigma_{12} = -\mu\sigma_{22} \tag{4.8}$$

μ being the coefficient of friction.

So in addition to the stress intensity factor N_{II} of $(4.4)_2$, we have from $(4.3)_2$

$$N_{II}^* = \frac{-2\mu}{\sigma_o \pi}\int_{\ell^*}^{\ell} \frac{\sigma_{22}(x)\,dx}{(\ell^2 - x^2)^{1/2}} \tag{4.9}$$

in the zone $\ell^* \leq |x| \leq \ell$. Inserting $\sigma_{22}(x)$ from (4.7), we find

$$N_{II}^* = \frac{-\mu A_2}{2}(\ell^2 - \ell^{*2})$$

which must be added to $(4.4)_2$ to account for the friction developed within the contact zone. Note that in deriving the above expression for N_{II}^* (4.5) has been used.

5. Experimental results

Tests were conducted on a commercial grade of polymethyl methacrylate (PMMA) with an elastic modulus of 0.5×10^6 lb/in^2 and a tensile strength of 8×10^3 lb/in^2. The specimens were 1.5 in. in diameter and approximately 0.125 in. thick. Details of the specimen preparation and testing procedures may be found in [8]. In addition, a series of three point bend tests were also conducted. To avoid errors which may be

produced in specimen preparation, the beam specimens were cut from 3.0 inch disks which were prepared in a fashion identical with the 1.5 in. disks. The results for the opening mode failure are given in Fig. 7. Here the normalized fracture load, $1/N_{IC}$, has been plotted. In Fig. 7, K_I has been normalized by using the average K_{IC} values from both the bend specimen and the disk test. As is evident, the experimental results follow the analytical results of this paper and those of Libatskii and Kovchik [5] quite closely with maximum deviation at short crack lengths.

Figure 8 presents results from the mode II fracture of PMMA. The results here show greater scatter than in mode I. This is most probably due to the precision required in orienting the specimen. Nevertheless, it is felt that the above results demonstrate the feasibility of using the disk test as a reliable method for obtaining K_{IC} and K_{IIC} fracture parameters. Additionally, the testing also demonstrates that the production of specimens of modest size with small ℓ/a ratios is feasible. This coupled

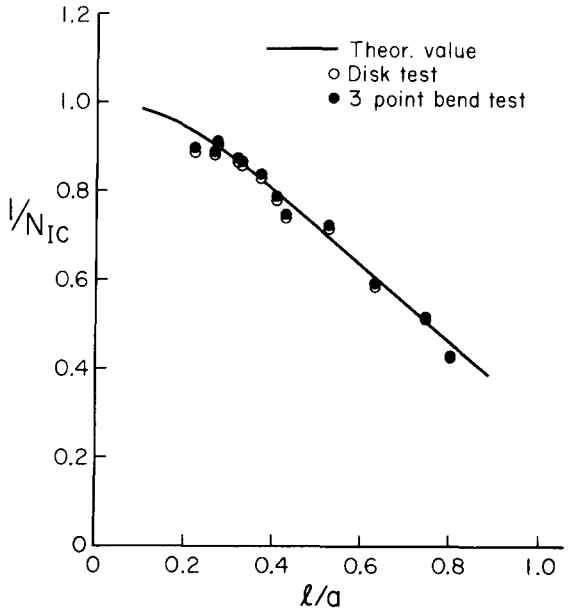

Figure 7. Critical Mode I load to fracture for PMMA.

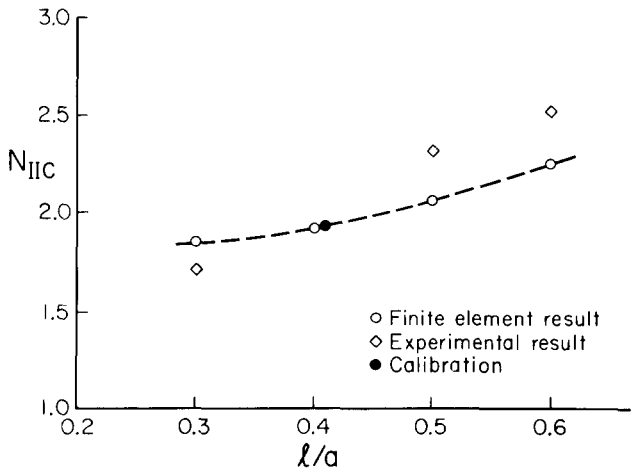

Figure 8. Critical Mode II stress intensity factor for PMMA.

with the analysis of Section 4 will allow a detailed study of the effects of combined mode fracture as well as an evaluation of the role of friction in the failure event.

6. Conclusions

The foregoing has presented an analysis of the cracked Brazilian disk test. The results of a numerical investigation yielded explicit formulae for the mixed mode stress intensity factors valid for any crack orientation. In addition, it was noted that for some angle the opening mode stress intensity factor became zero, and beyond this angle, the crack was closed. An approximate analysis was developed for short cracks and a scheme for the inclusion of friction was presented. Experiments were conducted on PMMA specimens, and it was demonstrated that modest size specimens could be produced with short crack lengths which yield reliable results. Thus, it is possible to analyze and investigate the problem of combined mode fracture using the cracked Brazil disk test.

Acknowledgment

The authors would like to thank the Air Force Office of Scientific Research for its financial support through the course of this work and M.L. Williams for his help and encouragement.

REFERENCES

[1] J. Eftis, N. Subramonian and H. Liebowitz, *Engineering Fracture Mechanics* 9 (1977) 189–210.
[2] J. Eftis, N. Subramonian and H. Liebowitz, *Engineering Fracture Mechanics* 9 (1977) 753–764.
[3] J. Eftis and N. Subramonian, *Engineering Fracture Mechanics* 10 (1978) 43–67.
[4] J.L. Swedlow, in *Cracks and Fracture, ASTM STP* 601 (1976) 506–521.
[5] L.L. Libatskii and S.E. Kovchik, *Soviet Materials Science* 3 (1967) 334–339.
[6] S.Ya. Yarema and G.S. Krestin, *Soviet Materials Science* 2 (1966) 7–10.
[7] H. Awaji and S. Sato, *Journal of Engineering Materials and Technology* 100 (1978) 175–182.
[8] J. Sanchez, Application of the Disk Test to Mode I-II Fracture Analysis, MS Thesis, Mechanical Engineering Department, University of Pittsburgh, Pittsburgh, PA (1979).
[9] D.L. Jones and D.B. Chisholm, *Engineering Fracture Mechanics* 7 (1975) 261–270.
[10] D.B. Chisholm and D.L. Jones, *Experimental Mechanics* 17 (1977) 7–13.
[11] C. Atkinson, *International Journal of Engineering Science* 10 (1972) 45–71.
[12] C. Atkinson, *International Journal of Engineering Science* 10 (1972) 127–136.
[13] P. Tong, T.H.H. Pian, and S.J. Lasry, *International Journal for Numerical Methods in Engineering* 7 (1973) 297–308.
[14] S.P. Timoshenko and J.N. Goodier, *Theory of Elasticity*, Third Edition, McGraw-Hill, New York (1970).
[15] E.G. Coker and L.N.G. Filon, *A Treatise on Photo-Elasticity*, Cambridge University Press, London (1931).

Appendix

Following [14, 15], the stresses relative to a cylindrical polar coordinate system ρ, θ, located at the center of the disk are*

$$\bar{\sigma}_{\rho\rho} = \frac{2P}{\pi a}\left[\frac{1}{2} - \frac{\left(1-\frac{\rho}{a}\cos\theta\right)\left(\cos\theta-\frac{\rho}{a}\right)^2}{\left(1+\frac{\rho^2}{a^2}-2\frac{\rho}{a}\cos\theta\right)^2} - \frac{\left(1+\frac{\rho}{a}\cos\theta\right)\left(\cos\theta+\frac{\rho}{a}\right)^2}{\left(1+\frac{\rho^2}{a^2}+2\frac{\rho}{a}\cos\theta\right)^2}\right]$$

* These expressions are due to Prof. R.J. Erdlac, Dept. of Mechanical Engineering, University of Pittsburgh

$$\bar{\sigma}_{\theta\theta} = \frac{2P}{\pi a}\left[\frac{1}{2} - \frac{\left(1-\frac{\rho}{a}\cos\theta\right)\sin^2\theta}{\left(1+\frac{\rho^2}{a^2}-2\frac{\rho}{a}\cos\theta\right)^2} - \frac{\left(1+\frac{\rho}{a}\cos\theta\right)\sin^2\theta}{\left(1+\frac{\rho^2}{a^2}+2\frac{\rho}{a}\cos\theta\right)^2}\right] \tag{A.1}$$

$$\bar{\sigma}_{\rho\theta} = \frac{2P}{\pi a}\left[\frac{\left(1-\frac{\rho}{a}\cos\theta\right)\left(\cos\theta-\frac{\rho}{a}\right)\sin\theta}{\left(1+\frac{\rho^2}{a^2}-2\frac{\rho}{a}\cos\theta\right)^2} + \frac{\left(1+\frac{\rho}{a}\cos\theta\right)\left(\cos\theta+\frac{\rho}{a}\right)\sin\theta}{\left(1+\frac{\rho^2}{a^2}+2\frac{\rho}{a}\cos\theta\right)^2}\right].$$

These may be expanded in a power series in ρ/a to give for $\bar{\sigma}_{\theta\theta}$ and $\bar{\sigma}_{\rho\theta}$

$$\bar{\sigma}_{\theta\theta} = \frac{P}{\pi a}\sum_{i=1}^{n} A_i(\theta)\left(\frac{\rho}{a}\right)^{2i-2}$$

$$\bar{\sigma}_{\rho\theta} = \frac{2P\sin 2\theta}{\pi a}\sum_{i=1}^{n} B_i(\theta)\left(\frac{\rho}{a}\right)^{2i-2}$$

where $A_1(\theta)$ to $A_5(\theta)$ and $B_1(\theta)$ to $B_5(\theta)$ are given in Table 2.

RÉSUMÉ

On a procédé à une analyse de l'essai du disque brésilien fissuré. Des résultats explicites sont fournis pour les facteurs d'intensité de contrainte relatifs à une fissure alignée dans une direction quelconque par rapport à un point de la charge appliquée. On considère diverses approximations et on montre qu'une approximation d'une fissure courte simplifiée permet d'assurer une exactitude pour des valeurs de $\ell/a \leq 0{,}3$ (ℓ est la longueur de la fissure et a le rayon du disque). Pour certains angles, on trouve que la fermeture de la fissure peut se produire et en première étape, on prend en compte l'effet de la friction pour de tels cas en utilisant cette approximation de fissure courte. Enfin, des résultats expérimentaux sont présentés en vue de confirmer et élucider l'utilisation de cette géométrie d'éprouvette dans le problème d'un mode de rupture combinée.